Journal of Instrumentation

PAPER

A hybrid muon detector design with RPC and plastic scintillator for the experiment at the Super Tau-Charm Facility

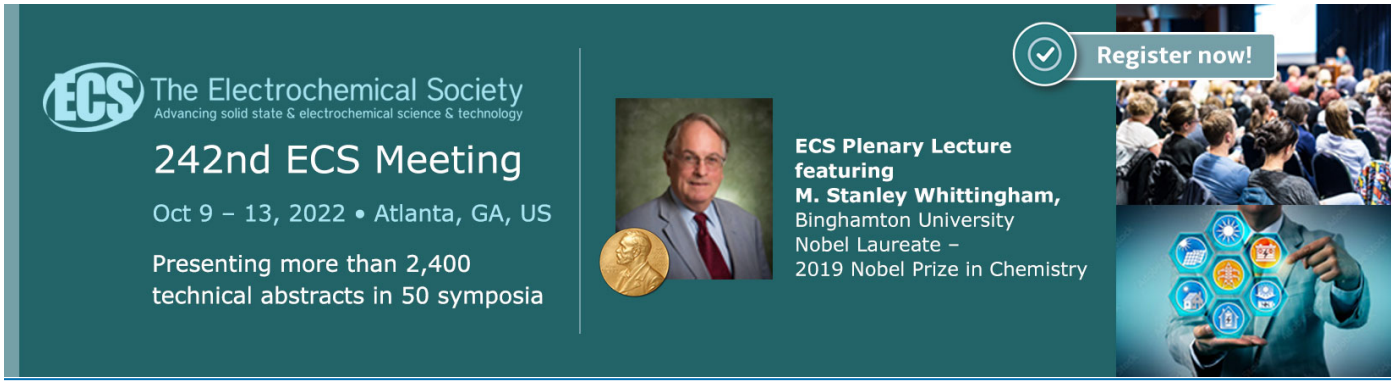

Published by IOP Publishing for Sissa Medialab

Received: *April 17, 2021*
Revised: *August 7, 2021*
Accepted: *August 31, 2021*
Published: *September 20, 2021*

A hybrid muon detector design with RPC and plastic scintillator for the experiment at the Super Tau-Charm Facility

Z. Fang, Y. Liu, H. Shi, J. Liu* and M. Shao

State Key Laboratory of Particle Detection and Electronics, University of Science and Technology of China, Hefei 230026, China

Department of Modern Physics, University of Science and Technology of China, Hefei 230026, China

E-mail: liujianb@ustc.edu.cn

Abstract: The Super Tau-Charm Facility (STCF) is a high-luminosity electron-positron collider project proposed in China. STCF acts as a natural extension of the BEPCII collider. The peak luminosity of STCF is over 50 times higher than that of the BEPCII, greatly benefitting tau-charm physics research. However, it demands a high-performance detector system. To obtain an optimal balance of the $\mu^{\pm}$ identification efficiency and the rejection of charged hadron background, while maintaining a reasonable overall cost, a hybrid muon detector design consisting of three layers of bakelite-RPCs and seven layers of scintillator strips is proposed for the experiment at the STCF. Simulations using the Geant4 package indicate that, in the beam-induced background predicted for the STCF experiment, the identification efficiency for $\mu^{\pm}$ with momenta exceeding 0.8 GeV/c can be higher than 95%, with a 97% $\pi^{\pm}$ rejection rate. The identification efficiency for neutrons that are not detected by the electromagnetic calorimeter exceeds 95% for a background rejection rate of 97%. These results demonstrate that the hybrid muon detector design can meet the demands for muon detection in the STCF experiment.

Keywords: Large detector systems for particle and astroparticle physics; Hybrid detectors

*Corresponding author.

https://doi.org/10.1088/1748-0221/16/09/P09022

2021 JINST 16 P09022

Contents

2021 JINST 16 P09022

1 Introduction

The Beijing Electron Positron Collider (BEPC) and its upgraded version BEPCII have operated in the tau-charm energy region in China for decades [1, 2]. To continue exploring the rich spectrum of physics in the tau-charm energy region after BEPCII, the Super Tau-Charm Facility (STCF) has been proposed as a natural successor. The design luminosity of $0.5 \times 10^{35}/\text{cm}^2/\text{s}$ [3] is almost two orders of magnitude higher than that of the BEPCII.

With increasing radius from the beamline, the proposed STCF detector will consist of an inner tracking detector, a main drift chamber, a time-of-flight detector, an electromagnetic calorimeter (ECAL), and a muon detector. A solenoidal magnet is installed between the ECAL and the muon detector. The muon detector (MUD) is the outermost part of the detector and provides $\mu^{\pm}$ identification in the presence of significant $\pi^{\pm}$ background. It can also be used for neutral hadron identification. The high luminosity of the STCF is expected to significantly benefit tau-charm physics research; however, it also generates a significantly higher level of beam-induced background [4], necessitating a MUD design with high rate capability and excellent background

suppression power. A resistive plate chamber (RPC)-based design was used for the muon detector at the Babar [5], BESIII [6], and BELLE [7] experiments with a luminosity ranging from 10^{33} to $10^{34}/\mathrm{cm}^2/\mathrm{s}$. Upgrade studies for the BELLEII experiment demonstrated that a muon detector based on the traditional glass-RPC cannot function effectively in a high-rate environment with a luminosity higher than $10^{34}/\mathrm{cm}^2/\mathrm{s}$ [8]. The glass RPCs in the Endcap and the first two layers of the Barrel of the BELLE muon detector were therefore replaced with scintillator strips [9, 10].

The momenta of final state $\mu^{\pm}$ and $\pi^{\pm}$ produced in electron-positron collisions at the STCF experiment are mostly below 2.0 GeV/c [11], as shown in figure 1. Because of ECAL and solenoid material preceding the MUD, the $\mu^{\pm}$ with momentum less than 0.4 GeV/c cannot be detected by the MUD. According to the demands from the STCF physics program [12], the $\mu^{\pm}$ detection challenge lies in the low-momentum region (<0.7 GeV/c), where $\mu^{\pm}$ have a short detector track length. It is easier to identify high-momentum $\mu^{\pm}$ when they have deep or full penetration in the MUD.

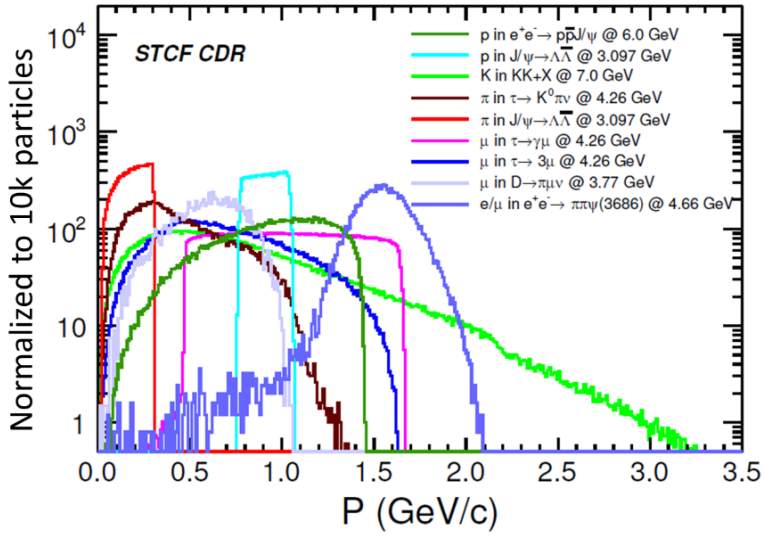

Figure 1. MC truth-level momentum distributions for charged particles in several benchmark processes at STCF. Each processes is normalized to 10K particles.

Considering the importance of identifying low-momentum $\mu^{\pm}$ in the STCF experiment, caution should be exercised when using the plastic scintillator in the high-background regions of the MUD. Plastic scintillator detectors in the MUD allow a high counting rate capability. However, it can also lead to additional in-time background hits. This is because the plastic scintillator has high sensitivity to low-energy secondary photons and neutrons produced in the beam-induced background. In particular, $\mu^{\pm}$ of momentum below 0.7 GeV/c penetrate at most four layers of the MUD, where the background is highest. For this reason, the use of plastic scintillator for the inner layers of the MUD would deteriorate the purity of the identified low momentum $\mu^{\pm}$.

As a result, the design of the MUD should be optimized to achieve a balance between the rate capability and the identification of low-momentum $\mu^{\pm}$. Consequently, a hybrid muon detector design that combines bakelite-RPC with plastic scintillator is proposed for the STCF. Details regarding this design, the optimization process, and the particle identification performance are presented in this paper.

2021 JINST 16 P09022

2 STCF MUD detector

The detector used as the MUD in the electron-positron collider must realize good particle detection performance over a $\sim 1000\,\mathrm{m}^2$ area, at acceptable cost. Hence, the bakelite-RPC and the plastic scintillator are appropriate choices. The bakelite-RPC, which operates in the avalanche mode, has a counting rate capability of approximately $10\,\mathrm{kHz/cm}^2$ [13], and it also offers the advantage of low background sensitivity. The plastic scintillator has been proven to be an efficient detector of $\mu^{\pm}$, $\pi^{\pm}$, and neutral hadrons. Compared with the bakelite-RPC, the plastic scintillator is more sensitive to photons and neutrons, conducive to achieving a higher neutral hadron detection efficiency. However, it suffers from extreme background hits.

To evaluate the influence of the background, the full simulation of the background in STCF MUD is performed using Geant4, including luminosity-related (radiative Bhabha scattering and two photon process) and beam-related (Touschek effect, Coulomb scattering, and bremsstrahlung) backgrounds. In this research, Geant4 [14] version 10.05.p01 is used, and the G4NDL4.5 library is also used for simulating neutron-related reactions. The physical list in the Geant4 simulation is QGSP_BERT_HP, with an energy cut of 990 eV for electron/positron/photon, and a default cut-off of 700 µm for other particles. Such a cut-off is similar to the common setting in FLUKA [15], and is expected to meet the simulation requirements of this study. Figure 2 shows the simulated background counting rate in the MUD, at full STCF luminosity, indicating that the rate of the plastic scintillator-based MUD is approximately 10.7 times higher than that of the RPC-based MUD. This is because the main background sources in the MUD are secondary photons and neutrons. Hence, the plastic scintillator achieves a higher counting rate owing to its higher sensitivity to these particles.

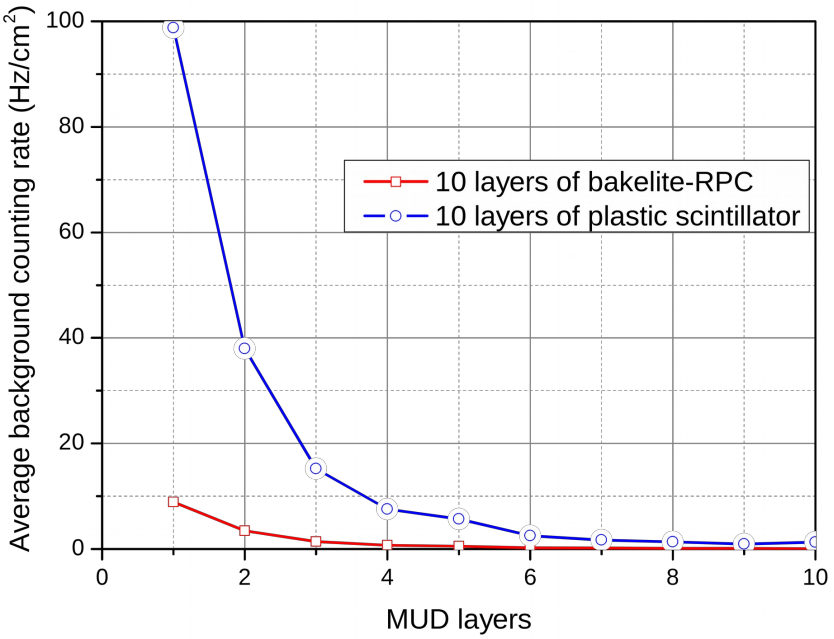

Figure 2. Geant4-simulated background counting rate in Barrel MUD, at full luminosity of STCF.

Figure 3 (a) shows the Geant4-simulated $\mu^{\pm}$ detection efficiency as a function of momentum, with and without background. The $\mu^{\pm}$ identification algorithm is described in section 4. As

2021 JINST 16 P09022

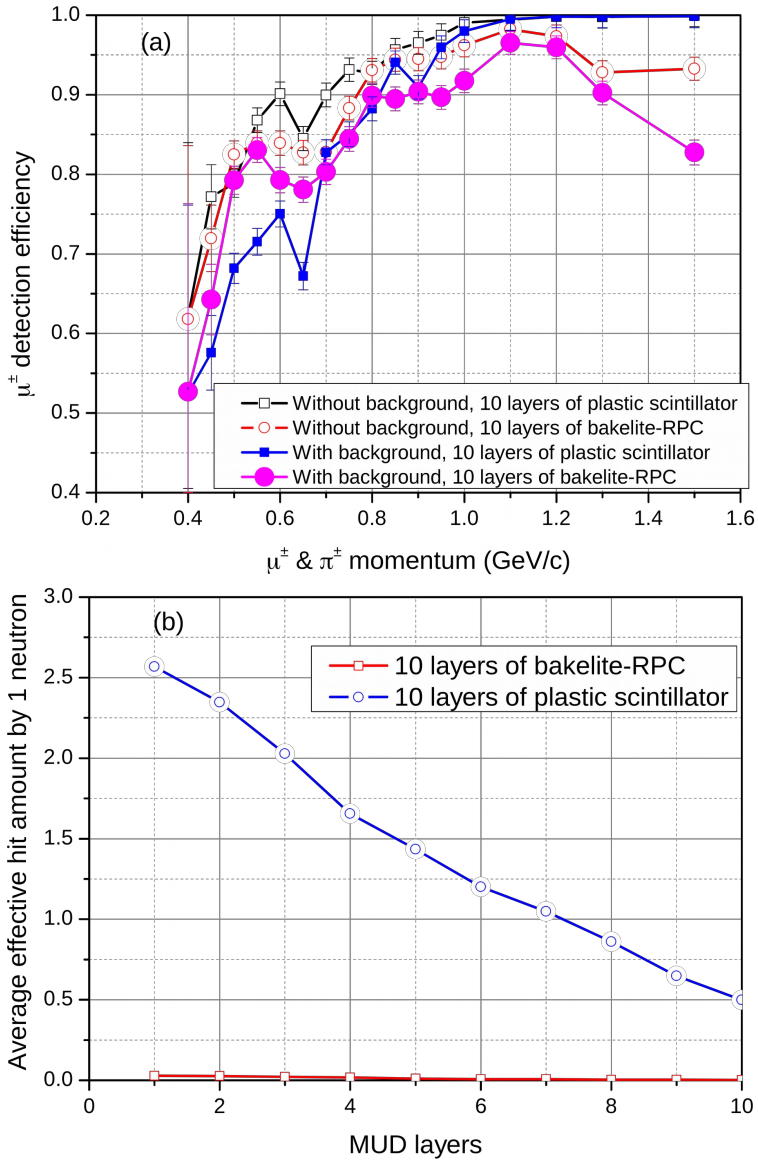

Figure 3. (a) $\mu^{\pm}$ detection efficiency curve @ $\pi^{\pm}$ rejection rate = 97% with or without background, in the direction of $\theta = 90°$ and $\varphi = 90°$ (θ: polar angle, φ: azimuth angle). (b) Average number of recorded hits per MUD layer from a neutron produced in STCF collisions.

is evident, with background, the $\mu^{\pm}$ detection efficiency curve of the plastic scintillator decreases sharply in the momentum range of 0.4 to 0.7 GeV/c, due to the influence of the high-level background. Nonetheless, the plastic scintillator exhibits a better $\mu^{\pm}$ identification performance in the high-momentum range, where the background level is low, as shown in figure 2. By contrast, the bakelite-RPC has better background suppression power in the low-momentum region. Figure 3 (b) shows the average number of recorded hits from a neutron produced at the STCF, in each MUD layer. This indicates that the neutron detection efficiency of the plastic scintillator is approximately 110 times higher than that of the bakelite-RPC.

2021 JINST 16 P09022

As the consequence, there exists a tradeoff between the particle detection efficiency and the background suppression power in the MUD design. An MUD composed entirely of bakelite-RPC or plastic scintillator is unsuitable, considering the luminosity level and the performance requirements of STCF. Therefore, a hybrid MUD design with both detectors could achieve better performance.

In the STCF, low-momentum $\mu^{\pm}$ can only generate signals in the first two to four layers of the MUD, where the background contribution is high. Consequently, the bakelite-RPCs are set on the inner side to detect low-momentum $\mu^{\pm}/\pi^{\pm}$ with a high S/B (signal/background) ratio. The plastic scintillators are then arranged on the outer side, which is responsible for detecting $\mu^{\pm}/\pi^{\pm}$ with momentum greater than 0.7 GeV/c at a low background level. For the neutral hadron detection, the plastic scintillator layers can realize effective measurements. Meanwhile, the bakelite-RPCs generate an "Empty Zone" (where the real signals caused by neutral hadrons are significantly less) to help separate the neutral and charged particles efficiently.

3 STCF MUD parameter optimization

3.1 MUD design

Figure 4 shows a schematic of the MUD design, following a performance optimization that is described in this section. The main parameters of the optimized design are listed in table 1. The optimization includes the structure and granularity of the Barrel and Endcap iron yokes, the location and granularity of the active detector layers, and the neutron background shielding.

The Barrel MUD is a hybrid design consisting of three bakelite-RPC layers, and seven polystyrene plastic scintillator layers with azimuthal granularity 4 cm, sandwiched between successive layers of the iron yoke. An equivalent Endcap MUD is complemented by neutron shielding and an inner Endcap yoke component ensuring the uniformity of the solenoidal magnetic field.

3.2 Optimization of the iron yoke setting and the number of detector layers

The $\mu^{\pm}$ momentum range in STCF is typically below 2.0 GeV, indicating that a total thickness of 50–60 cm for the iron yoke is sufficient to meet the demands of hadron showers. Optimized using Geant4 simulations, the total thickness of the iron yoke is set as 51 cm.

Additional detector layers in the MUD could help achieve better performance. Figure 5 illustrates the $\mu^{\pm}$ detection efficiency curves for different detector layer settings and the yoke with a thickness of 51 cm. In the simulation, nine to eleven layers are applied and evaluated. The result indicates that ten or eleven layers in the detector could afford a higher and smoother $\mu^{\pm}$ detection efficiency curve. Considering the detector complexity and manufacturing costs, the MUD baseline design adopts ten layers in the detector.

The thickness of the iron yoke between two MUD layers from the inner to outer sides should be gradually increased. However, rapid increments in the thickness, such as doubling the yoke thickness in a single step, should be avoided to prevent a significant drop in the $\mu^{\pm}$ detection efficiency. Based on Geant4 simulations, the thickness of the yoke is set as 4, 4, 4.5, 4.5, 6, 6, 6, 8, and 8 cm from the inner to outer sides. On the outer surface of the MUD, a 15 cm-thick iron layer is arranged as protection for the entire system. The Endcap MUD has an additional layer with a 4 cm-thick yoke plate inside the innermost detector, in order to compensate for the lack of a solenoid in the Endcap part.

2021 JINST 16 P09022

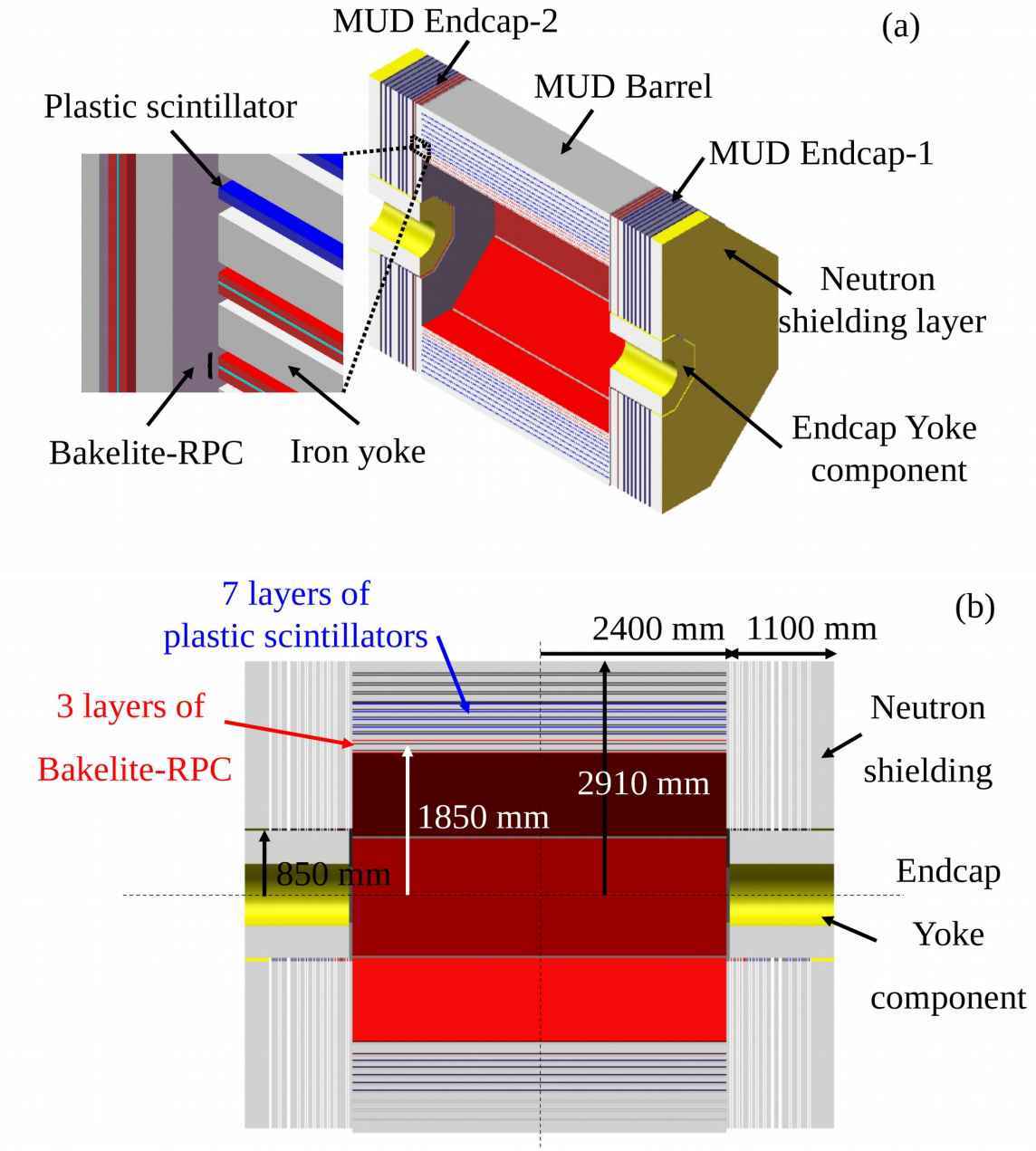

Figure 4. Schematic of the MUD design. (a) The half-section view of the MUD, and the partial enlarged view of the sandwiched-placement of bakelite-RPC, plastic scintillator, and iron yoke. (b) The cutaway view of MUD, and the setting of main structural parameters.

3.3 Optimization of the arrangement of the bakelite-RPC and plastic scintillator

The arrangement of the bakelite-RPC and plastic scintillator in the ten layers affects the performance of the MUD. On the one hand, the plastic scintillator has higher robustness and higher detection efficiency for high-momentum $\mu^{\pm}$. On the other hand, the Geant4 simulation indicates that the bakelite-RPC has better performance in detecting low-momentum $\mu^{\pm}$ in the high-background region of the MUD.

2021 JINST 16 P09022

Table 1. Structural parameters of the MUD. R_{in} and R_{out} are the inner and outer radii of the Barrel MUD, respectively, including the 15 cm-thick iron plate shielding outside the detector system. R_e is the inner radius of the Endcap MUD. L_{Barrel} and T_{Endcap} are the lengths of the Barrel and Endcap MUD along the z-direction, respectively. The dimensions of the composite neutron shielding, and the Endcap yoke component are not included.

Parameter	Value
R_{in} [cm]	185
R_{out} [cm]	291
R_e [cm]	85
L_{Barrel} [cm]	480
T_{Endcap} [cm]	107
Segmentation in φ	8
Number of detector layers	10
Iron yoke thickness [cm]	4/4/4.5/4.5/6/6/6/8/8
(λ=16.77 cm)	Total: 51 cm, 3.04 λ
Solid angle	79.2% $\times 4\pi$ in Barrel
	14.8% $\times 4\pi$ in Endcap
	94% $\times 4\pi$ in total
Total area [m^2]	$\sim$ 717 in Barrel
	$\sim$ 520 in Endcap
	$\sim$ 1237 in total

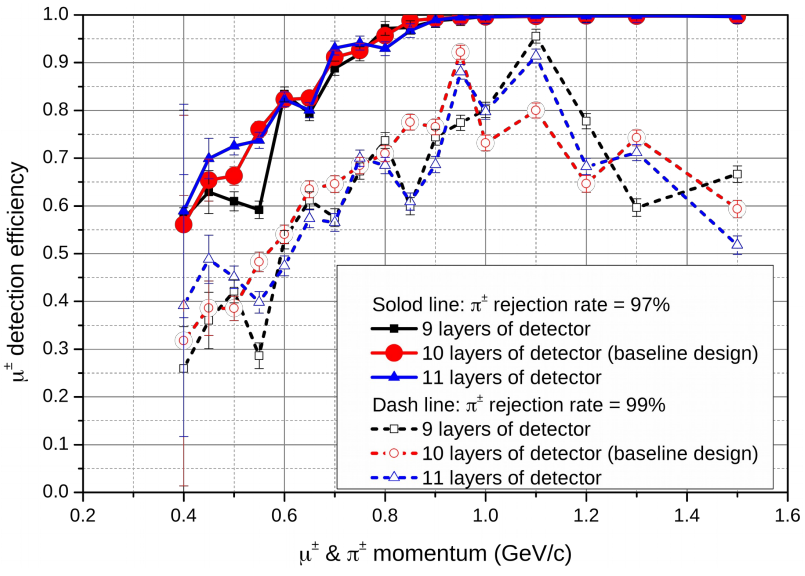

Figure 5. Geant4-simulated $\mu^{\pm}$ detection efficiency curves for different layers in the detector, with a constant total yoke thickness.

Figure 6 shows the Geant4-simulated $\mu^{\pm}$ detection efficiency as a function of momentum, for different MUD layouts, and respectively 97% and 99% $\pi^{\pm}$ rejection at full STCF luminosity. The MUD designs with two, three, or four layers of the bakelite-RPC exhibit similar $\mu^{\pm}/\pi^{\pm}$ separation power under the current luminosity and background level.

To suppress the influence of background, the optimized situation requires the background counting rates in the 1st layer of the bakelite-RPC and the 1st layer of plastic scintillator to be similar. According to figure 2, three layers of the bakelite-RPC are sufficient to cover the high-background region, indicating that an additional bakelite-RPC layer is unnecessary. For the design with two layers of the bakelite-RPC, a high counting rate and significant interference may occur in the 3rd (plastic scintillator) layer due to the potential fluctuations in the background level or the future upgrades of STCF. As a result, the hybrid MUD design with three layers of the bakelite-RPC and seven layers of plastic scintillator is considered as the optimal choice.

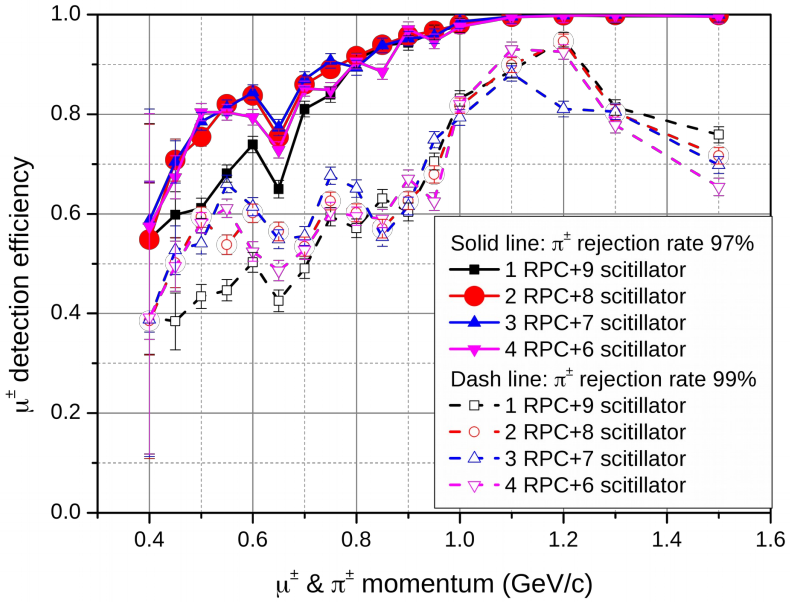

Figure 6. $\mu^{\pm}$ detection efficiency curves with different combinations of bakelite-RPC and plastic scintillator in the MUD design along the direction of $\theta = 90°$ and $\varphi = 90°$ (θ: polar angle, φ: azimuth angle) under the background.

3.4 Granularity of detector

The granularity is determined by the readout strip pitch of the bakelite-RPC and the size of the plastic scintillator strips. Physics simulations of the measurement precision for reconstructed $\mu^{\pm}$ indicate that a spatial resolution of 1–2 cm is required in the MUD, equivalent to a detector granularity of 3.5 - 7 cm. Figure 7 presents the simulated $\mu^{\pm}$ detection efficiency curves with different granularities, indicating similar particle detection performances. As a lower granularity implies additional electronic channels, both the readout strip pitch of the bakelite-RPC and the width of the plastic scintillator strips are chosen to be 4 cm. In this case, a balance between the spatial resolution and the number of readout channels can be realized. The maximum lengths of

2021 JINST 16 P09022

the bakelite-RPC module and plastic scintillator strips are set to approximately 1.1 m and 2.8 m, respectively. This could be realized using existing detector manufacturing technologies [10]. In this design, the number of readout channels in the MUD is estimated to be approximately 19000 for the bakelite-RPC and approximately 21840 for the plastic scintillator.

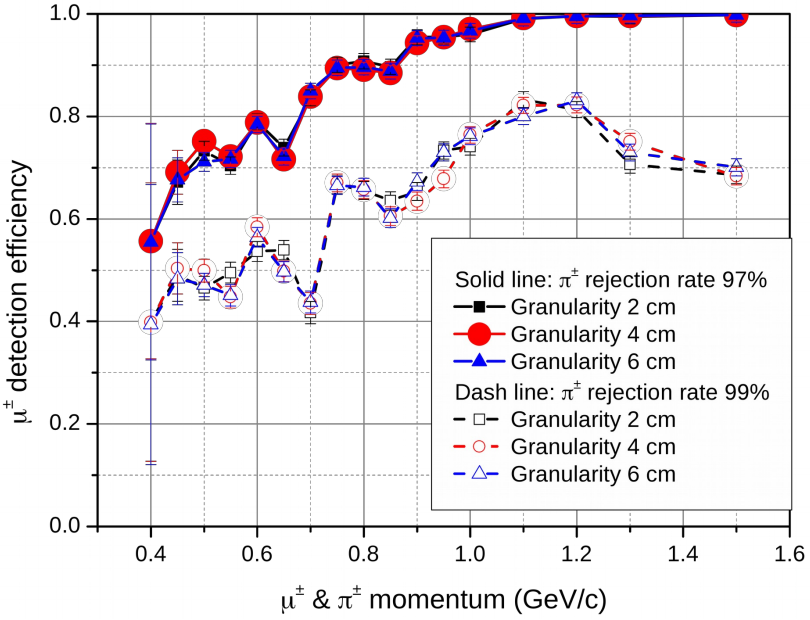

Figure 7. Geant4-simulated $\mu^{\pm}$ detection efficiency with different granularities along the zenith direction.

3.5 Background neutron shielding and Endcap yoke setting

Previous studies by the BELLEII collaboration [16] indicated a concern from neutrons produced by GeV-level electrons and positrons of the exterior beam background. This neutron background leads to additional background hits in the MUD. In this design, to suppress the background caused by exterior neutrons, the outer surface of Endcap MUD is covered with a 15 cm-thick composite neutron shielding. The outer part of the neutron shielding is composed of 5 cm-thick lead, whereas the inner part is 10 cm-thick boron-doped polyethylene (10 wt.% of nat-boron). The lead moderates fast neutrons to the energy of approximately 1 MeV, and the boron-doped polyethylene subsequently moderates the neutrons to the thermal region and absorbs them through the reaction of n (^{10}B, ^{7}Li) α.

A Geant4 simulation demonstrated that the 15 cm-thick composite neutron shielding could decrease the MUD hits by approximately 90% for neutrons with a kinetic energy less than 1 MeV, as shown in figure 8. The background simulation also provides the total counting rate in the MUD, as shown in table 2. The neutron shielding reduces the resulting neutron background in the Endcap MUD by one to two magnitudes, adequate for the STCF.

A cylindrical yoke component is arranged between the beamline and the Endcap MUD; this is designed to ensure a uniform magnet field in the STCF detector system. The thickness of this cylindrical yoke is approximately 40–45 cm. Geant4 simulations indicate that the yoke provides the similar background suppression capability similar to that of the composite shielding.

2021 JINST 16 P09022

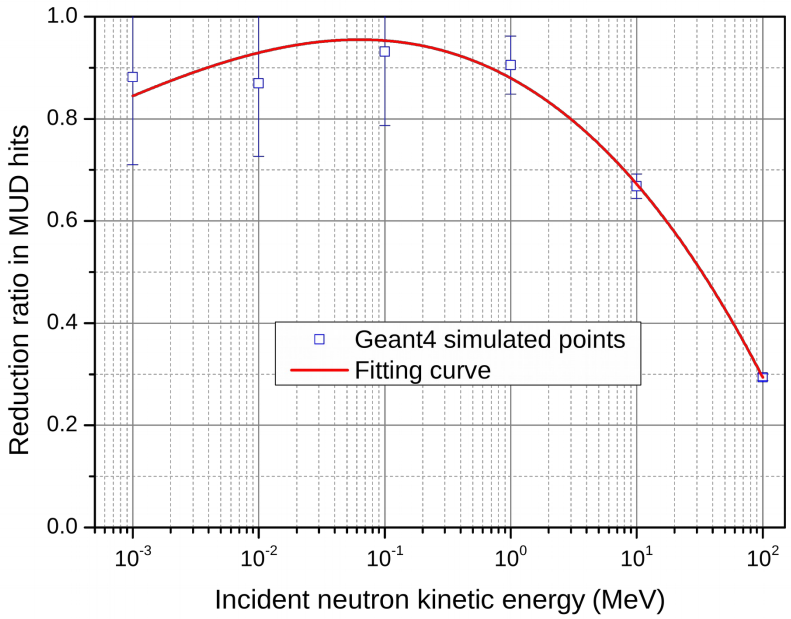

Figure 8. Geant4-simulated reduction ratio in MUD hits, when the composite neutron shielding is arranged in the Endcap MUD.

Table 2. Simulated background total counting rate in the MUD.

	Barrel		Endcap	
	3 layers Bakelite-RPC	7 layers plastic scintillator	3 layers Bakelite-RPC	7 layers plastic s scintillator
With neutron shielding (Hz)	6.16×10^6	1.14×10^7	3.73×10^6	2.61×10^7
Without neutron shielding (Hz)	7.31×10^6	1.37×10^7	1.32×10^7	9.18×10^8
Background remaining ratio	84.3%	83.2%	28.3%	2.8%

4 Particle identification algorithm

The primary purpose of an MUD is to identify $\mu^{\pm}$ with high efficiency and with high purity following the rejection of the dominant $\pi^{\pm}$ background. The secondary purpose is to serve as the auxiliary neutral hadron detector. To realize an efficient particle identification ability, the signals in the main drift chamber (MDC), the ECAL, and the MUD are separately processed via a track/cluster locating algorithm. The track of $\mu^{\pm}$ or $\pi^{\pm}$ penetrates the MDC and the ECAL before entering the MUD, forming a set of continuous hits in these detectors. Neutral hadrons, such as neutrons and K_{L}, only generate cluster-like signals in the ECAL or the MUD when showered. By matching the hits in the three detector systems, the potential track-like and cluster-like MUD hits can be separated to a certain extent and analyzed using special boosted decision tree (BDT) algorithms.

2021 JINST 16 P09022

4.1 $\mu^{\pm}$ identification algorithm

In the STCF, the main interference in $\mu^{\pm}$ detection is caused by $\pi^{\pm}$, and both of them can generate a set of continuous hits along the penetration path. The $\pi^{\pm}$ may shower via strong interactions, resulting in a shorter track length and additional hits around the shower point. As a result, the size and shape parameters of the track in detector systems could be used as effective BDT parameters, as shown in table 3. The BDT algorithm for the MUD track consists of five subroutines: hit sorting, track locating with MDC extrapolation, background removing, track fitting, and BDT calculation. In the BDT algorithm, the time window is limited to 100 ns in order to suppress the background counting rate. Meanwhile, the multiple hits at the same scintillator strip are merged into one hit if the simulated detected time difference is within 10 ns.

Table 3. BDT parameters used in the $\mu^{\pm}$ identification algorithm.

Parameter	Definition
E_{ecal}	Energy deposited in ECAL
$L_{\mathrm{distancetoip}}$	Distance from track's last hit to IP
T_{time}	Detected time of track in the first detector layer
$N_{\mathrm{maxhitlayer}}$	Layer number that has the most hits
$N_{\mathrm{lastlayer}}$	Layer number that has the last hit
$L_{\mathrm{meandistance}}$	Mean distance from each two neighborhood hits in the track
N_{totalhit}	Total number of hits in 10 layers of the detector
$N_{\mathrm{first3hit}}$	Number of hits in first 3 layers of the detector
N_{last7hit}	Number of hits in last 7 layers of the detector
N_{noisehit}	Number of hits identified as the background
A_{theta}	Reconstructed polar angle of the track in the R-Z plane
T_{TCtype}	Judged as track or cluster
$Q_{\mathrm{trackquality}}$	Quality of the track

4.2 Neutral hadron identification algorithm

In the STCF, the MUD can support the ECAL in neutral hadron detection and identification, such as the neutron/anti-neutron and K_{L}, from the dominant photon background. With momenta mostly below 1.6 GeV/c, more than 60% of the neutral hadrons shower in the 30 cm-thick ECAL (pure CsI) [18]. The other 40% can penetrate ECAL and deposit a small amount of energy (less than 40 MeV), thereby requiring efficient detection in the MUD.

The BDT algorithm for neutral hadron identification is executed in the following order: hit sorting, cluster locating, background removing, cluster fitting, and BDT calculation. In the BDT algorithm, the time window is set to be 300 ns, which is sufficient to collect the slow signals produced via secondary neutrons. Table 4 presents the optimized BDT parameters used in neutral hadron identification.

2021 JINST 16 P09022

Table 4. BDT parameters used in the neutral hadron identification algorithm.

Parameter	Definition
$E_{\rm ecal}$	Energy deposited in ECAL
$L_{\rm distancetoip}$	Distance from cluster's last hit to IP
$T_{\rm time}$	Detected time of cluster in the first detector layer
$N_{\rm maxhitlayer}$	Layer number that has the most hits
$N_{\rm lastlayer}$	Layer number that has the last hit
$L_{\rm meandistance}$	Mean distance from each two neighborhood hits in the MUD cluster
$N_{\rm totalhit}$	Total number of hits in 10 layers of the detector
$N_{\rm first3hit}$	Number of hits in first 3 layers of the detector
$N_{\rm last7hit}$	Number of hits in last 7 layers of the detector
$N_{\rm noisehit}$	Number of hits identified as the background
$L_{\rm meanscintillatordistance}$	Mean distance from point of scintillator hit to the center of scintillator hits
$L_{\rm stdscintillatordistance}$	Standard deviation of distance from the point of scintillator hit to the center of scintillator hits
$A_{\rm theta}$	Reconstructed polar angle of the track in the R-Z plane
$T_{\rm TCtype}$	Judged as track or cluster
$N_{\rm mdc}$	Number of hits in MDC
Necal	Number of hits in ECAL
$R_{1/3}$	ECAL energy deposition ratio between the central crystal and the 3×3 array
$R_{1/5}$	ECAL energy deposition ratio between the central crystal and the 5×5 array
$R_{2/3}$	ECAL energy deposition ratio between the 2×2 and the 3×3 array
$R_{2/5}$	ECAL energy deposition ratio between the 2×2 and the 5×5 array
$R_{3/5}$	ECAL energy deposition ratio between the 3×3 and the 5×5 array
SOM_3	Second-order moment of energy deposition in the 3×3 ECAL crystal array
SOM_5	Second-order moment of energy deposition in the 5×5 ECAL crystal array

4.3 Evaluation of BDT algorithms

To evaluate the quality of the BDT algorithm, the multi-layer perceptron (MLP) and likelihood methods are used to differentiate the $\mu^{\pm}$ from $\pi^{\pm}$, considering an example of 1 GeV/c. Figure 9

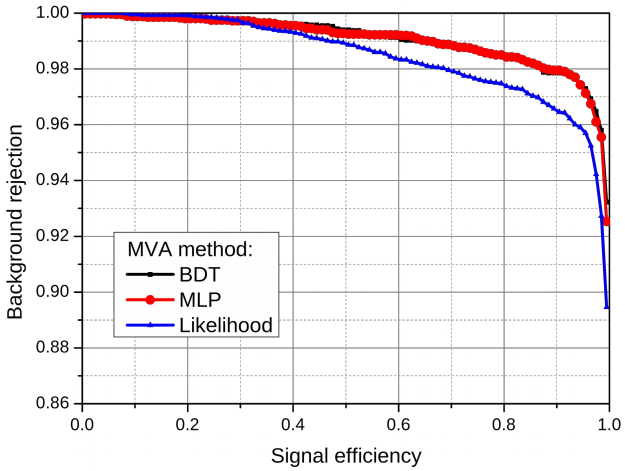

Figure 9. Background rejection rate versus signal efficiency of the BDT, MLP, and likelihood algorithms.

2021 JINST 16 P09022

shows the background rejection rate versus the signal efficiency for the three algorithms. Evidently, the BDT and MLP have similar particle identification efficiencies, while the likelihood method has a slightly inferior performance. Figure 10 presents the algorithm responses and the Kolmogorov-Smirnov (K-S) test results. For all the algorithms, the K-S test probability exceeds 0.05, indicating that the three algorithms are not over-trained.

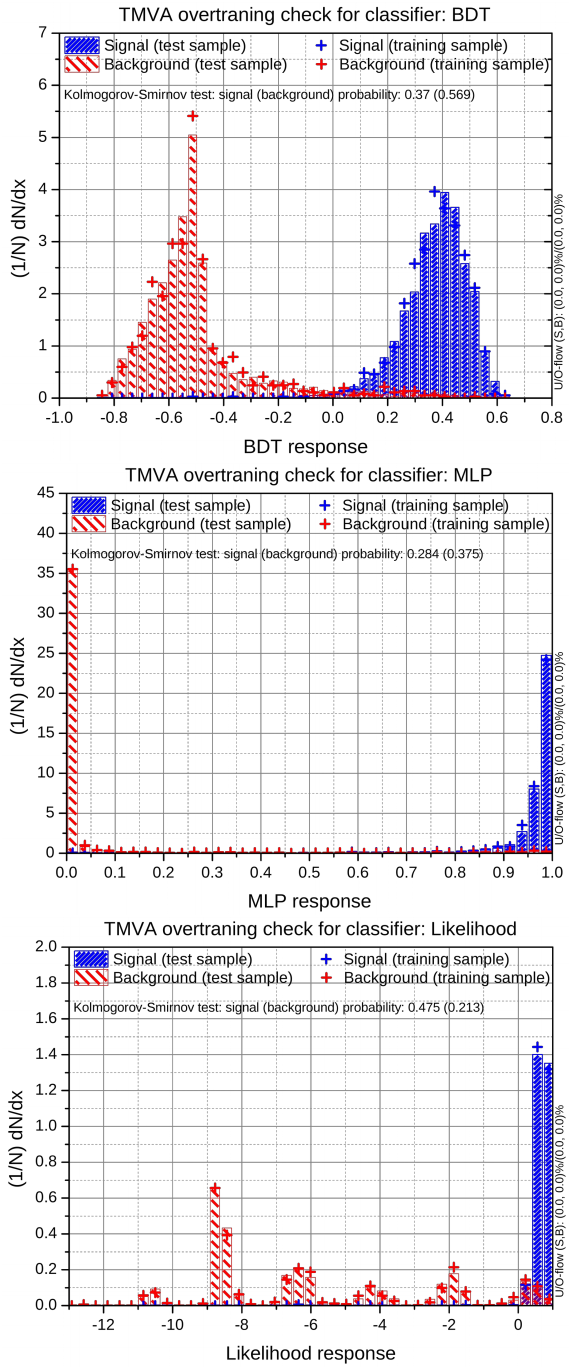

Figure 10. Algorithm responses for the signal and background, and Kolmogorov-Smirnov test results, with BDT, MLP, and likelihood algorithms.

5 Particle identification simulations

5.1 $\mu^{\pm}$ identification ability

Figure 11 shows the simulated $\mu^{\pm}$ detection efficiency curves of the STCF baseline MUD design and the BESIII-like MUD design with no background and the same BDT algorithm. A significant increase in the $\mu^{\pm}$ detection efficiency can be observed in the momentum range of $[0.65, 1.5]$ GeV/c owing to a thicker yoke and the optimized detector setting. Figure 12 presents the distribution of the $\mu^{\pm}$ identification efficiency of this design in the momentum range of $[0, 2.5]$ GeV/c and polar angle range of $[20°, 160°]$, considering a $\pi^{\pm}$ rejection rate of 97% and background influence.

In the simulation, the momentum range is divided in steps of 50 MeV/c; therefore, in each cycle of the simulation, the range of the $\mu^{\pm}$ track in the MUD exhibits a fluctuation of approximately 3.6 cm. Thus, the $\mu^{\pm}$ detection efficiency may decrease for a thickness of 4–8 cm of one-layer yoke in the MUD. This is because in one cycle of the simulation, a portion of the $\mu^{\pm}$ may penetrate N layers of the detector, while the remaining portion penetrates N+1 layers. Therefore, in the BDT algorithm, it is more difficult to separate $\mu^{\pm}$ that penetrates N layers of the detector from the $\pi^{\pm}$, which reduces the average efficiency of the entire bin.

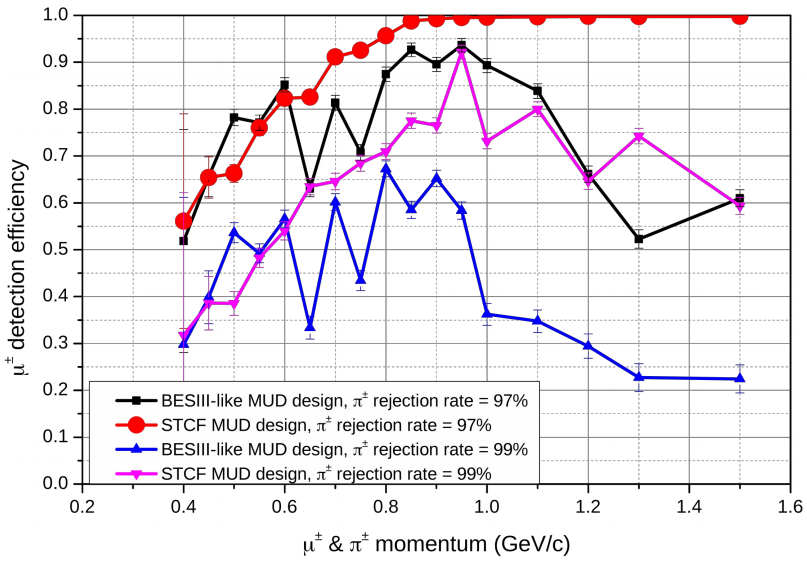

Figure 11. Comparison between STCF baseline MUD design and BESIII-like MUD design with the same BDT algorithm in the zenith direction and no background included.

The $\mu^{\pm}$ detection efficiency curves exhibit a peak point. In the zenith direction, this point is approximately 1.2 GeV/c, where the $\pi^{\pm}$ penetrate the outermost layer of the MUD. Thus, the $\pi^{\pm}$ shower probability remains constant, and it is approximately 98.1% when the transverse momentum exceeds 1.2 GeV/c (the total equivalent thickness of ECAL and MUD is 4 times the nuclear interaction length). When the $\pi^{\pm}$rejection rate is less than the $\pi^{\pm}$ shower probability, the $\mu^{\pm}$ detection efficiency could be close to 100% (i.e., $\pi^{\pm}$ rejection rate = 97%). However, if the $\pi^{\pm}$rejection rate is larger than the $\pi^{\pm}$ shower probability, such as 99%, some $\mu^{\pm}$ will inevitably be lost when distinguishing $\mu^{\pm}$ from the $\pi^{\pm}$ without a shower, leading to decreased $\mu^{\pm}$ detection efficiency.

2021 JINST 16 P09022

Figure 13 illustrates the feature importance of the main BDT parameters, indicating that the number of Not-in-Track hits (N_{noisehit}) is most effective for $\mu^{\pm}$ identification. This is because most $\pi^{\pm}$ terminate as a hadron shower, resulting in hits distributed over a large area and forming a cluster rather than a clear track.

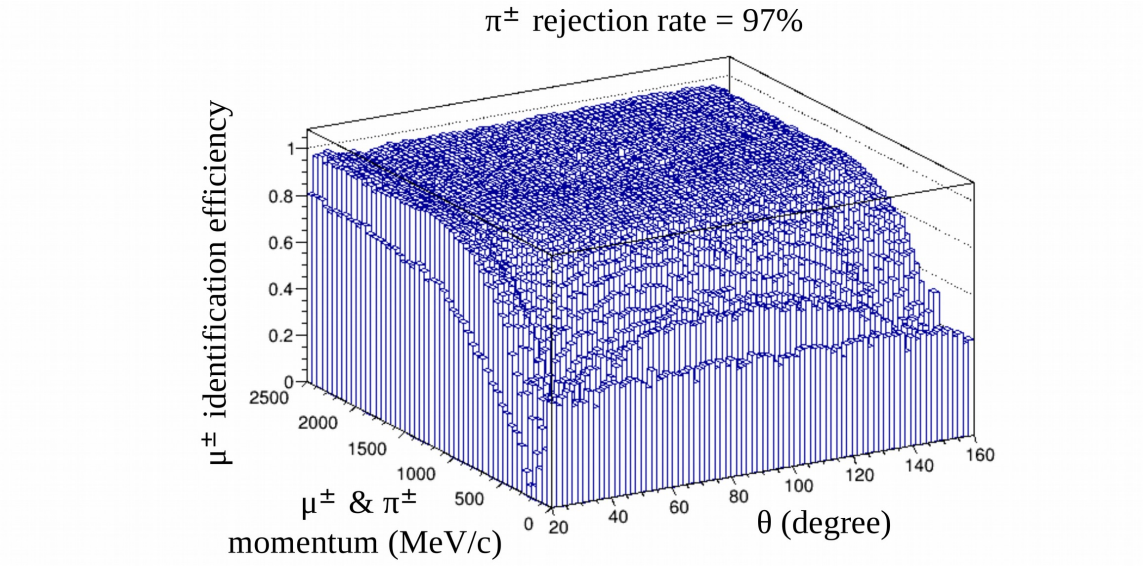

Figure 12. The Geant4 simulated $\mu^{\pm}$ identification efficiency as a function of the particle momentum and polar angle, at the nominal peak STCF luminosity. The rejection rate for a $\pi^{\pm}$ mis-identified as a $\mu^{\pm}$ is 97%.

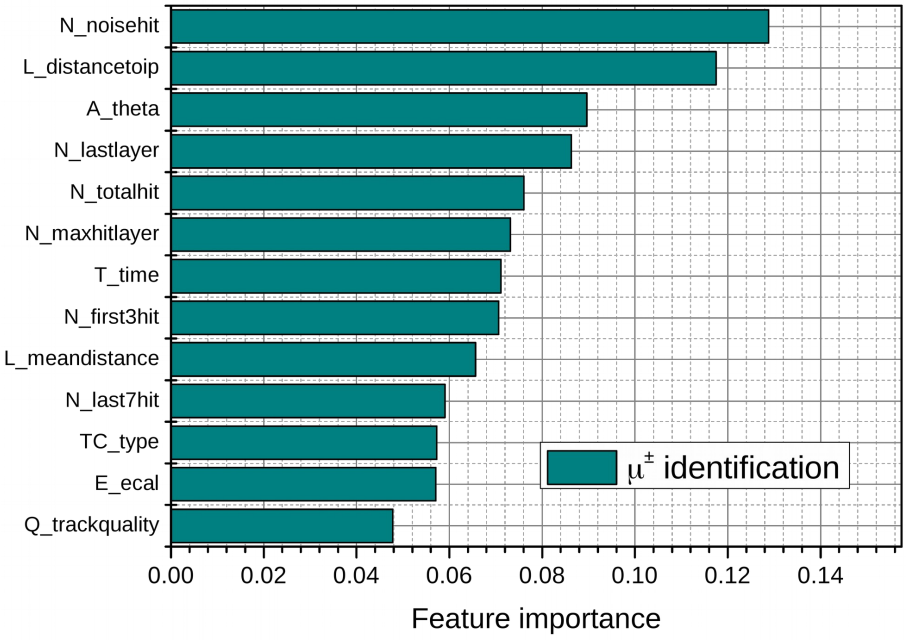

Figure 13. Feature importance of BDT parameters used in $\mu^{\pm}$ identification.

5.2 Neutral hadron detection and identification ability

Neutral hadron detection in the STCF detector system is simulated using Geant4, at the nominal peak STCF luminosity. The momentum distribution of the neutral hadron is generated by the physics processes of interest. The simulation result indicates that 40% of the neutral hadrons deposit less than 40 MeV of energy in ECAL, leading to a considerably lower identification efficiency in the presence of background. However, for these same neutral hadrons, the MUD shows a high detection efficiency, as indicated in figure 14. It is evident that, if the neutrons survive after penetrating the ECAL (or depositing a small amount of energy in the ECAL), the detection efficiency of MUD can increase to 95% for a photon rejection rate of 97%. This is because the secondary photons and neutrons can be directly detected via plastic scintillators in the MUD when the surviving neutral hadron showers in the yoke. Figure 15 shows the variation of the neutron and K_L identification efficiency in the polar angle range of $[20°, 160°]$, momentum range of $[0, 1.6]$ GeV/c and $[0, 1.8]$ GeV/c, respectively. The simulation results demonstrate that the MUD, as designed, effectively complements the ECAL in identifying neutral hadrons that may not be detected by the ECAL.

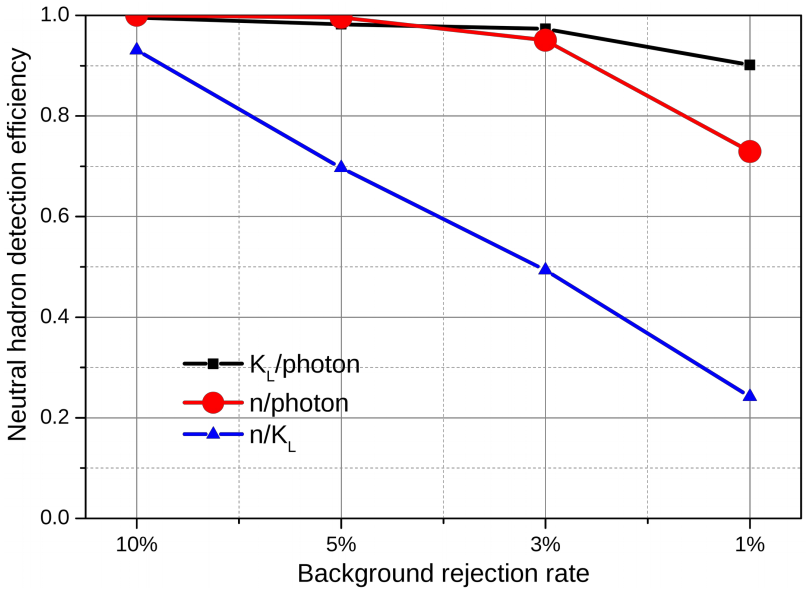

Figure 14. Detection efficiency curve with different categories of neutrons along the zenith direction.

Figure 16 shows the feature importance of the BDT parameters in the separation of neutron/photon. It is clear that the Energy Deposition in ECAL (E_{ecal}) helps to efficiently distinguish neutrons because the E_{dep} in the ECAL of neutron is limited to less than 40 MeV. The number of Not-in-Cluster hits ($N_{noisehit}$) also shows a high feature importance, owing to the high sensitivity of the plastic scintillators in the MUD to secondary photons and neutrons in the hadron shower.

6 Discussion

Plastic scintillator has emerged as an important alternative choice for MUD detection layers, given its good detection efficiency for neutral hadrons and $\mu^{\pm}$, high counting rate capability, and ease of

2021 JINST 16 P09022

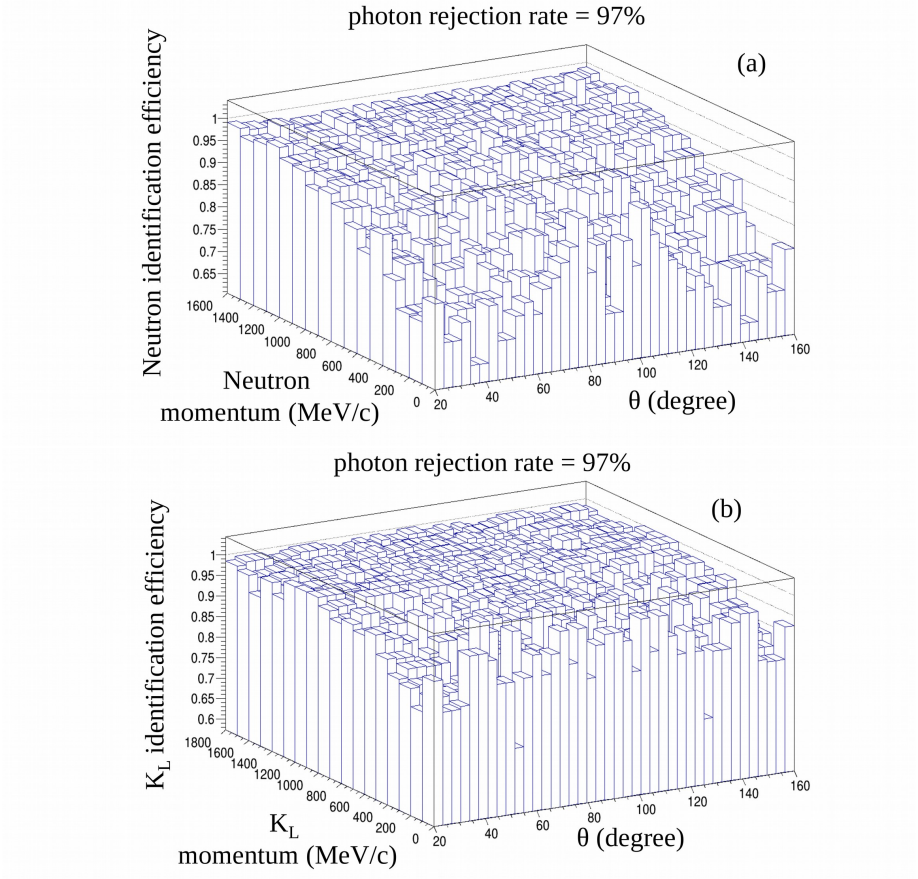

Figure 15. The Geant4 simulated neutron (a) and $K_{\rm L}$ (b) identification efficiency as a function of the particle momentum and polar angle, at the nominal peak STCF luminosity. The rejection rate for a photon mis-identified as a neutron or $K_{\rm L}$ is 97%.

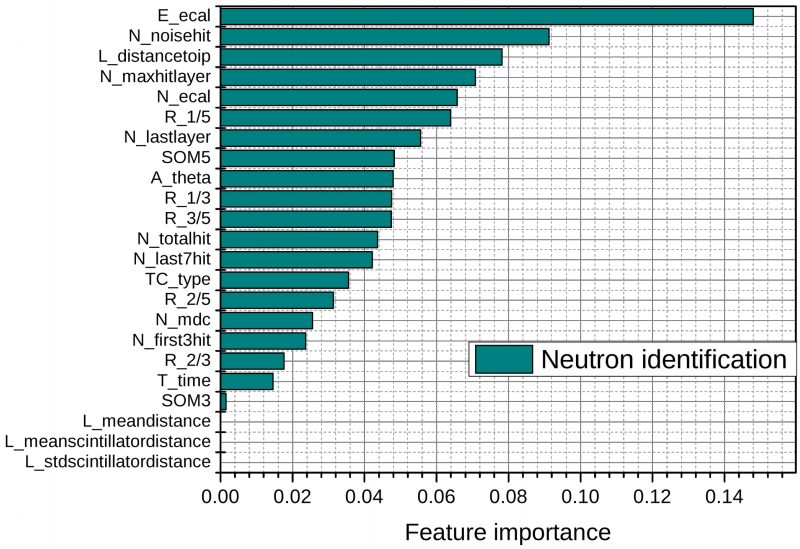

Figure 16. Feature importance of BDT parameters used in neutral hadron identification.

maintenance. To meet requirements of counting rate with increased luminosity, plastic scintillator is being considered for upgrades of the BELLEII MUD [9], in particular for the Endcap MUD and the first two layers of the Barrel MUD. Additionally, some researchers have proposed an MUD design entirely composed of plastic scintillator strips. However, the background counting rate when using plastic scintillator remains an issue with increased luminosity. In the hybrid MUD design proposed in this paper, the composite detector system is arranged by setting the bakelite-RPC in the first three layers of the MUD where the background is high and by arranging the plastic scintillators on the outer side. In this manner, the advantages of both the bakelite-RPC and plastic scintillator can be utilized: low background sensitivity of bakelite-RPC, and the high neutral hadron detection efficiency of plastic scintillator. Thus, this novel hybrid MUD design is more suitable for the newly proposed STCF.

With the physical processes in STCF, neutrons are always generated with anti-neutrons, such as in the reactions $e^+e^- \to n\bar{n}$ and $e^+e^- \to \gamma n\bar{n}$. Anti-neutrons are easier to identify owing to the high annihilation probability [19]. This could help to distinguish neutrons from K_L and achieve efficient neutral hadron identification capability.

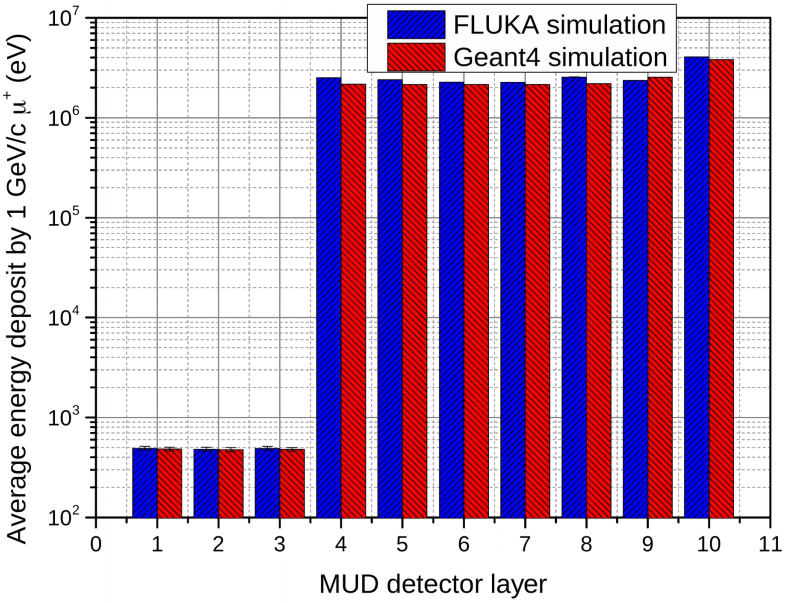

Figure 17. Average energy deposit by 1 GeV/c μ^+ in 10 layers of the MUD along the zenith direction.

To evaluate the accuracy of the Geant4 simulations, FLUKA (version 2021.2.0) is also used for simulations. FLUKA is highly efficient in simulating the statistic distribution over an area, such as doses and fluxes. However, using FLUKA for event by event particle identification is inefficient. Therefore, FLUKA is used to simulate the average energy deposit in each layer of the MUD, and the energy spectra. Figure 17 presents the average energy loss by a μ^+ of 1 GeV/c in each of the ten MUD layers, for both FLUKA and Geant4. The simulated FLUKA energy loss is slightly higher, but the results are similar. Figure 18 shows the normalized energy loss of 0.5 GeV/c neutrons in the first layer of the plastic scintillator. These simulation results indicate that Geant4 and FLUKA achieve similar simulation performances for hadrons and neutral particles in the STCF

2021 JINST 16 P09022

detector system. However, a difference of approximately 10% exists in the statistics of the energy deposit; this is attributed to the differences of the simulation methods and the dE/dx data for the two types of software.

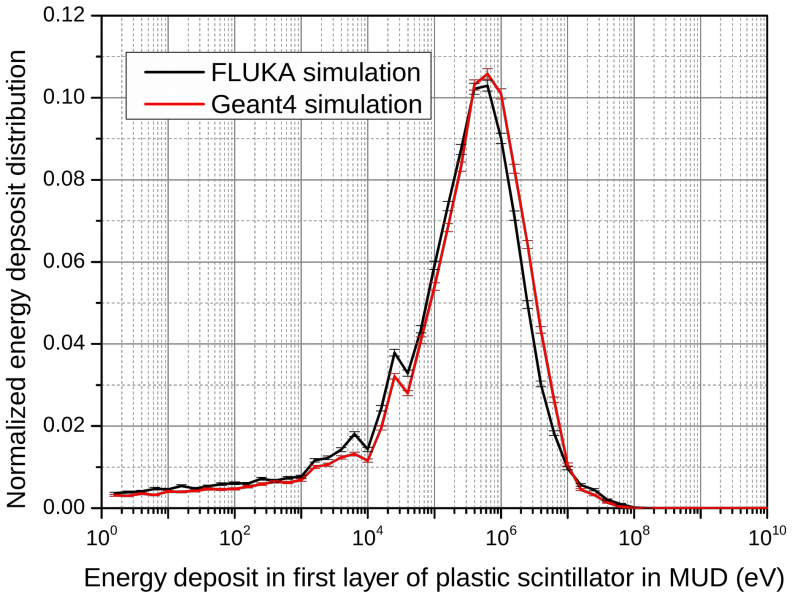

Figure 18. Normalized energy deposit spectra of 0.5 GeV/c neutrons in the first layer of the plastic scintillator along the zenith direction.

Previous performance studies of the BELLE MUD detector [20] can be used to compare with the STCF MUD design. In BELLE, the average $\mu^{\pm}$ identification efficiency and the $\pi^{\pm}$ fake rate are 89% and 1.4%, respectively, with the standard selection criterion of 0.9 between 1.0 to 3.0 GeV/c [20]. The STCF MUD has a performance similar to that of BELLE KLM in the range of 1.0 to 1.5 GeV/c (average $\mu^{\pm}$ detection efficiency of 88% under a $\pi^{\pm}$ fake rate of 1.6%). However, there are certain differences in other momentum regions. In the range below 1.0 GeV/c, the STCF MUD design has a higher $\mu^{\pm}$ identification efficiency because the inner layers of the iron yoke are thinner, resulting in additional hits detected by $\mu^{\pm}$ and more precise measurements of the end point of the track. In the range above 1.5 GeV/c, the $\mu^{\pm}$ identification efficiency of STCF MUD is lower than that of BELLE owing to the difference in the physical requirements of the $\mu^{\pm}$ detector design. In BELLE, the target $\mu^{\pm}$ momentum range is 0.6–3.0 GeV/c, so the KLM contains 14 layers of the detector and 70.5 cm thick iron yoke. In the STCF, the physical requirement indicates a $\mu^{\pm}$ momentum range of approximately 2.0 GeV/c, which implies that fewer detector layers and a thinner iron yoke are reasonable.

7 Conclusion

The STCF experiment is designed to be a viable successor to BEPCII, and can provide unique data on tau-charm and hadron physics with a luminosity 50 times that of BEPCII. The STCF MUD detector is designed for the detection of $\mu^{\pm}$ with high efficiency and purity, as well as to be used as an auxiliary neutral hadron detector. The proposed MUD design is a tradeoff between detector

2021 JINST 16 P09022

performance and volume owing to its 10-layer detector design. To ensure a balance of excellent $\mu^{\pm}$ detection efficiency, with excellent charged hadron rejection, a new hybrid MUD design comprising three layers of bakelite-RPC and seven layers of the scintillator detector is proposed. Geant4 simulation results indicate that, using this MUD design, the momentum detection threshold of $\mu^{\pm}$ can be decreased to approximately 0.45 GeV/c owing to the low background sensitivity in the first three layers of the bakelite-RPC. Thus, an acceptable $\mu^{\pm}$ detection efficiency with a $\pi^{\pm}$ rejection rate of 97% or 99% can be obtained.

An excellent identification efficiency for neutral hadrons is also possible because of the seven layers of the plastic scintillator. Geant4 simulations indicate that the detection efficiency of the MUD can be increased to 95% at a photon rejection rate of 97%, when the neutral hadron deposit is less than 40 MeV (which can be difficult to identify by the ECAL). This result proves that the MUD can be the good supplement of ECAL for neutral hadron detection. In conclusion, this new hybrid MUD design can achieve reliable $\mu^{\pm}$ and neutral hadron identification under the peak luminosity of STCF and could thus be the optimal choice for STCF MUDs.

Acknowledgments

This work was supported by the Double First-Class university project foundation of USTC; the CAS Center for Excellence in Particle Physics (CCEPP).

References

[1] J. Wang et al., *Status and performance of BEPCII*, in *Proceedings of the 1st International Particle Accelerator Conference*, Kyoto, Japan, 23–28 May 2010, pp. 2359-2363.

[2] D.M. Asner et al., *Physics at BES-III*, *Int. J. Mod. Phys. A* **24** (2009) S1 [arXiv:0809.1869].

[3] G. Huang, *The Super Tau Charm Factory Plan in China*, talk given at the *15th International Workshop on Tau Lepton Physics*, Amsterdam, The Netherlands, 24–28 September 2018, https://indico.cern.ch/event/632562/.

[4] J. Liu, *Detector Concepts for the Super Tau-Charm Facility in China*, talk given at the *Joint Workshop on Future Tau-Charm Factories*, LAL, Orsay, France, 4–7 December 2018, https://indico.ijclab.in2p3.fr/event/4902/.

[5] F. Anulli et al., *The muon and neutral hadron detector for BaBar*, *Nucl. Instrum. Meth. A* **409** (1998) 542.

[6] J. Zhang et al., *The BESIII muon identification system*, *Nucl. Instrum. Meth. A* **614** (2010) 196.

[7] Y. Hoshi, N. Kikuchi, T. Nagamine, K. Neichi and A. Yamaguchi, *Performance of the endcap RPC in the Belle detector under high luminosity operation of the KEKB accelerator*, *Nucl. Phys. B Proc. Suppl.* **158** (2006) 190.

[8] Belle-II collaboration, *Detectors for extreme luminosity: Belle II*, *Nucl. Instrum. Meth. A* **907** (2018) 46.

[9] T. Aushev et al., *A scintillator based endcap K_L and muon detector for the Belle II experiment*, *Nucl. Instrum. Meth. A* **789** (2015) 134 [arXiv:1406.3267].

[10] T. Uglov, *K-long and muon system for the Belle II experiment*, 2017 *JINST* **12** C07035.

2021 JINST 16 P09022

[11] H. Peng, *Status of the STCF Project in China*, talk given at the *Joint Workshop on Future Charm-Tau Factory*, Moscow, Russia, 24–28 September 2019, https://c-tau.ru/indico/event/3/sessions/16/.

[12] X.-D. Shi, X.-R. Zhou, X.-S. Qin and H.-P. Peng, *A fast simulation package for STCF detector*, 2021 *JINST* **16** P03029 [arXiv:2011.01654].

[13] CEPC Study Group, *CEPC Conceptual Design Report: Volume 2 — Physics & Detector*, Tech. Rep., IHEP-CEPC-DR-2018-02, Geneva, Switzerland (2018) [arXiv:1811.10545].

[14] J. Allison et al., *Recent developments in Geant4*, *Nucl. Instrum. Meth. A* **835** (2016) 186.

[15] T.T. Böhlen, F. Cerutti, M.P.W. Chin, A. Fassò, A. Ferrari, P.G. Ortega et al., *The FLUKA Code: Developments and Challenges for High Energy and Medical Applications*, *Nucl. Data Sheets* **120** (2014) 211.

[16] Belle-II collaboration, *Belle II Technical Design Report*, arXiv:1011.0352.

[17] K. Abe, Y. Hoshi, T. Nagamine, K. Neichi, K. Onodera, T. Takahashi et al., *Neutron sensitivity of the endcap RPC modules in Belle detector*, *IEEE Trans. Nucl. Sci.* **50** (2003) 831.

[18] http://pdg.lbl.gov/2011/AtomicNuclearProperties/index.html.

[19] M. Astrua, E. Botta, T. Bressani, D. Calvo, C. Casalegno, A. Feliciello et al., *Antineutron nucleus annihilation cross-sections below 400-MeV/c*, *Nucl. Phys. A* **697** (2002) 209.

[20] A. Abashian et al., *Muon identification in the Belle experiment at KEKB*, *Nucl. Instrum. Meth. A* **491** (2002) 69.

2021 JINST 16 P09022